Original Article

^{18}F-FDG PET/CT imaging of pediatric peripheral neuroblastic tumor: a combined model to predict the International Neuroblastoma Pathology Classification

Luo-Dan Qian[1#], Li-Juan Feng[1#], Shu-Xin Zhang[1], Jun Liu[1], Jia-Liang Ren[2], Lei Liu[3], Hui Zhang[4], Jigang Yang[1]

[1]Nuclear Medicine Department, Beijing Friendship Hospital, Capital Medical University, Beijing, China; [2]GE Healthcare, Beijing, China; [3]Sinounion Medical Technology (Beijing) Co., Ltd., Beijing, China; [4]Department of Biomedical Engineering, School of Medicine, Tsinghua University, Beijing, China

Contributions: (I) Conception and design: J Yang, J Liu; (II) Administrative support: J Yang; (III) Provision of study materials or patients: LD Qian, LJ Feng, SX Zhang; (IV) Collection and assembly of data: LD Qian, LJ Feng; (V) Data analysis and interpretation: JL Ren, L Liu, H Zhang; (VI) Manuscript writing: All authors; (VII) Final approval of manuscript: All authors.

[#]These authors contributed equally to this work and should be considered as co-first authors.

Correspondence to: Dr. Jigang Yang, MD, PhD. Nuclear Medicine Department, Beijing Friendship Hospital, Capital Medical University, No. 95, Yong'an Road, Beijing 100050, China. Email: yangjigang@ccmu.edu.cn.

Background: The aim of this study was to evaluate the effect of a model combining a 18F-fluorodeoxyglucose positron emission tomography/computed tomography (^{18}F-FDG PET/CT)-based radiomics signature with clinical factors in the preoperative prediction of the International Neuroblastoma Pathology Classification (INPC) type of pediatric peripheral neuroblastic tumor (pNT).

Methods: A total of 106 consecutive pediatric pNT patients confirmed by pathology were retrospectively analyzed. Significant features determined by multivariate logistic regression were retained to establish a clinical model (C-model), which included clinical parameters and PET/CT radiographic features. A radiomics model (R-model) was constructed on the basis of PET and CT images. A semiautomatic method was used for segmenting regions of interest. A total of 1,016 radiomics features were extracted. Univariate analysis and the least absolute shrinkage selection operator were then used to select significant features. The C-model was combined with the R-model to establish a combination model (RC-model). The predictive performance was validated by receiver operating characteristic (ROC) curve analysis, calibration curves, and decision curve analysis (DCA) in both the training cohort and validation cohort.

Results: The radiomics signature was constructed using 5 selected radiomics features. The RC-model, which was based on the 5 radiomics features and 3 clinical factors, showed better predictive performance compared with the C-model alone [area under the curve in the validation cohort: 0.908 *vs.* 0.803; accuracy: 0.903 *vs.* 0.710; sensitivity: 0.895 *vs.* 0.789; specificity: 0.917 *vs.* 0.583; net reclassification improvement (NRI) 0.439, 95% confidence interval (CI): 0.1047–0.773; P=0.01]. The calibration curve showed that the RC-model had goodness of fit, and DCA confirmed its clinical utility.

Conclusions: In this preliminary single-center retrospective study, an R-model based on ^{18}F-FDG PET/CT was shown to be promising in predicting INPC type in pediatric pNT, allowing for the noninvasive prediction of INPC and assisting in therapeutic strategies.

Keywords: Peripheral neuroblastic tumor (pNT); 18F-fluorodeoxyglucose positron emission tomography/computed tomography (^{18}F-FDG PET/CT); radiomics; International Neuroblastoma Pathology Classification (INPC)

Submitted Apr 08, 2022. Accepted for publication Sep 09, 2022. Published online Oct 10, 2022.
doi: 10.21037/qims-22-343
View this article at: https://dx.doi.org/10.21037/qims-22-343

Introduction

Peripheral neuroblastic tumor (pNT) is the most common extracranial solid tumor to occur in childhood. The International Neuroblastoma Pathology Classification (INPC) describes 4 categories of pNT: neuroblastoma; ganglioneuroblastoma, intermixed; ganglioneuroma; and ganglioneuroblastoma, nodular (1). According to the INPC classification, morphological features (degree of neuroblast differentiation and mitotic nuclear division index) as well as the patient's age at diagnosis are considered in the prognostic differentiation of pNT into favorable histology (FH) or unfavorable histology (UH) (1).

Pathology type based on the INPC is one of the most powerful prognostic factors for patients with pNT (2,3). For example, the 3-year event-free survival (EFS) rates of patients with FH and UH tumors have been reported to be 85% and 41%, respectively (2). The prognostic value of INPC type has also been validated in large collaborative group studies to identify specific groups of patients at risk who may benefit from improved treatment (4). In one study, patients with International Neuroblastoma Staging System (INSS) stage 1 and 2 diseases and FH had a significantly better prognosis than did patients with UH (EFS 90%±3% and 72%±7%, respectively; overall survival 99%±1% and 86%±5%, respectively) (5). The Children's Oncology Group (COG) also stratifies patients by age, *MYCN* gene status, INSS stage, ploidy, and tumor histology using the INPC criteria (3,6). Therefore, INPC type is important not only for exact diagnosis and adequate histological subclassification, but also as an index of COG risk stratification. Moreover, the INPC type is essential for the precision treatment of pNT patients (7). However, INPC type is defined by multiple indexes, including age at diagnosis, grade of neuroblast differentiation, mitosis-karyorrhexis index, and quantity of Schwannian stromal development (3), which may lead to a lack of complete agreement among different pathologists. Santiago *et al.* reported that the complete agreement rate between different pathologists was about 25.0% (7). Furthermore, the treatment of patients with neuroblastoma is based on preoperative risk stratification, and surgical treatment is not usually used first if the patient is at high risk preoperatively. Additionally, the patient's risk stratification may change during the course of treatment. Therefore, the noninvasive and real-time assessment of INPC classification has become increasingly vital. The process of INPC categorization is complicated, expensive, and invasive. INPC type is paramount in terms of providing information about pNT, and there is potential for clinicians to assess pNT biology noninvasively by using imaging characteristics (8). Advances in imaging methods, such as in 18F-fluorodeoxyglucose positron emission tomography/computed tomography (^{18}F-FDG PET/CT), may provide a new intersection between molecular oncology and radiology (9). ^{18}F-FDG PET/CT is an integrated imaging modality of PET and CT and is used for evaluating tumor heterogeneity to reflect metabolism, hypoxia, cellular proliferation, vascularization, necrosis, receptor expression, or inter/intracellular signaling pathways (10). Common metrics that can be derived from PET imaging data include the maximum standardized uptake value (SUVmax), metabolic tumor volume (MTV), and total lesion glycolysis (TLG = SUVmean × MTV), among others. Although PET parameters based on SUV are helpful for the grading of malignant tumors, they cannot reflect intratumoral heterogeneity through the spatial distribution of metabolic activity in the whole tumor (10).

Radiomics is an emerging field that has been successfully applied to cancer research. It involves the conversion of medical images into a high-dimensional mineable feature space through automated data characterization algorithms and has demonstrated its potential in identifying tumor phenotypes and the pathological grading of malignant tumors (11). Radiomics analysis of ^{18}F-FDG PET/CT has proven capable of predicting TERTp-mutation status in high-grade gliomas (12); microvascular invasion in hepatocellular carcinoma and intrahepatic cholangiocarcinoma (13); and hormone receptor distribution, proliferation rates, and lymph node and distant metastases in breast adenocarcinomas (14). However, there has been limited research in developing noninvasive machine-learning models to accurately predict INPC type in pNT preoperatively. Therefore, we hypothesized that radiomics features extracted from PET/CT images can reflect cellular and molecular information and predict the INPC type.

In this study, we collected ^{18}F-FDG PET/CT images and

INPC data with the aim to create a prediction model based on ^{18}F-FDG PET/CT radiomics features for predicting the INPC type and to verify whether the combination of clinical characteristics with the radiomics model can better predict the INPC type in pediatric pNT. We present the following article in accordance with the STARD (Standards for Reporting Diagnostic accuracy studies) reporting checklist (available at https://qims.amegroups.com/article/view/10.21037/qims-22-343/rc).

Methods

Patient data

A retrospective analysis of 139 consecutive pediatric patients newly diagnosed with pNT between March 2018 and November 2019 at Beijing Friendship Hospital, Capital Medical University, was conducted. The inclusion criteria were as follows: (I) pathologically confirmed pNT; (II) ≤18 years at first diagnosis; (III) complete PET/CT imaging data and clinical information (see below); and (IV) no cancer-related therapy (e.g., biopsy, radiotherapy, chemoradiotherapy, or surgery) before PET/CT imaging. Subsequently, 33 cases were excluded, including 20 cases without clinical information and 13 cases who had undergone cancer-related treatment by the first diagnosis. A total of 106 patients were included in this study (Figure S1). These patients were randomly divided into the training cohort and validation cohort at a ratio of 7:3. Two pathologists with 15 and 20 years of pediatric experience independently participated in the review. According to the INPC type, morphological features, and patient age, pediatric patients were classified as FH or UH by preoperative biopsy. The pathologists were blinded to the prior pathology report. If there was any disagreement, the final pathological result would be decided by two pathologists via discussion. The study conformed to the provisions of the Declaration of Helsinki (as revised in 2013). This retrospective study was approved by the Institutional Ethics Committee of Beijing Friendship Hospital, and individual consent for this retrospective analysis was waived.

^{18}F-FDG PET/CT imaging

All patients underwent PET/CT whole-body scans (Biograph mCT-64 PET/CT; Siemens) according to the European Association of Nuclear Medicine (EANM) guidelines (15,16). Prior to the scan, they were asked to fast for at least 6 h and to reduce high-intensity exercise for at least 24 h. ^{18}F-FDG 0.10–0.15 MBq/kg (provided by Beijing Atomic Technology Co., Ltd.) was injected intravenously 40–60 min before the PET/CT scan. A low-dose CT scan with anatomical reference and attenuation correction was first performed with a tube voltage of 120 kV and automatic tube current modulation. The CT imaging parameters were as follows: resolution 0.586 mm × 0.586 mm, slice thickness 2 mm, and matrix size 512×512. The whole-body CT scan was immediately followed by a PET scan for 2 min in each bed. The ordered subset expectation maximization (OSEM) algorithm with time of flight (TOF) was used to reconstruct the PET images. The PET imaging parameters were as follows: resolution 4.07 mm × 4.07 mm, slice thickness 3 mm, and matrix size 200×200.

Conventional clinical data

Clinical characteristics including patient age, gender, and serum levels of neuron-specific enolase (NSE), serum ferritin (SF), lactate dehydrogenase (LDH), vanillylmandelic acid (VMA), and homovanillic acid (HVA) were collected within 1 month of the FDG PET/CT scan.

PET/CT radiographic features: The International Neuroblastoma Risk Group Staging System (INRGSS) stage of each patient was evaluated according to the report published by the International Neuroblastoma Risk Group, and the largest lesion was analyzed in the presence of multiple lesions (14). Two experienced nuclear medicine physicians (with 10 and 5 years of experience in pediatric nuclear medicine), who were blinded to the histopathological diagnosis, independently reviewed the conventional images at a workstation (syngo.via, Siemens) and recorded the following lesion features: (I) INRGSS (17) L1, L2, stage M, and stage MS; (II) anatomical compartment; (III) infiltration across the midline (beyond the opposite side of the vertebral column, present or not); (IV) calcification (present or not); (V) and necrosis (present or not). The anatomical compartment of each tumor was classified as chest, abdomen, pelvis, or junction (tumor that extends into an adjacent compartment). All results were determined by consensus agreement between the two nuclear medicine physicians.

PET quantitative parameters and radiomics feature extraction and selection

The primary tumor delineation was performed using the

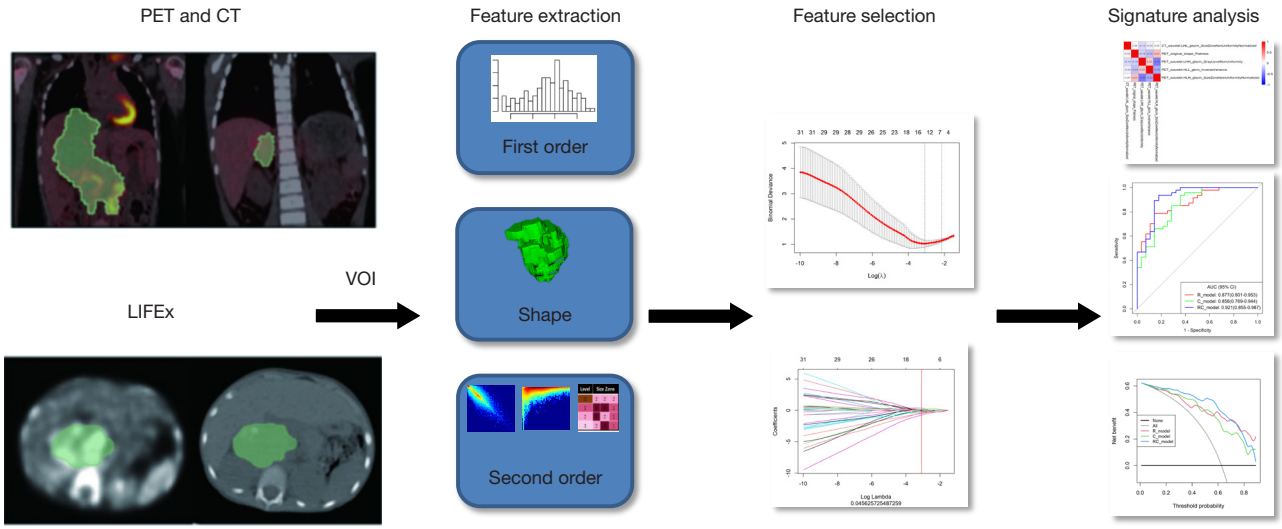

Figure 1 Radiomics signature workflow. PET, positron emission tomography; CT, computed tomography; VOI, volume of interest.

fixed SUV threshold method. According to the results of previous studies, 40% of SUVmax was set as the threshold for the images (18-20). In this method, 3D contours were drawn around voxels equal to or greater than 40% SUVmax. For a volume of interest (VOI) containing more than 1 cluster, the cluster which had maximum uptake intensity and volume was selected. Manual verification after automatic segmentation was performed, and special attention was paid to tumors located near the urinary bladder due to intense physiological urinary tracer activity. This step was negotiated by the 2 previous nuclear medicine physicians. It is common to perform preprocessing of the data to conform the voxel size of CT and PET data prior to feature extraction. Radiomics features of CT and PET images were calculated in the same VOI. In the above VOI, standard PET quantitative parameters were measured [SUVmax, MTV, and TLG (TLG = SUVmean × MTV)], and radiomics features were calculated by using LIFEx software (www.lifexsoft.org) (21), which only calculates radiomics features for VOIs of at least 64 voxels.

Establishment of the clinical and radiomics models

Univariate analysis was performed to compare the differences in clinical characteristics and PET/CT radiographic features between pNT patients with FH and UH in the training cohort. Significantly different variables were added to the multivariate logistic regression analysis. Based on the selected characteristics, a clinical model (C-model) was established. A total of 1,016 radiomics features were obtained from PET and CT images of the training cohort. To reduce overfitting or selection bias in our radiomics model, the feature selection procedure was performed as follows: (I) the Mann-Whitney U test retained features with P values less than 0.05; (II) correlation analysis was performed and features with a correlation coefficient greater than 0.9 were removed; (III) the least absolute shrinkage selection operator (LASSO) was used to explore the information features most relevant to the INPC type. Finally, the features with significant differences were screened to establish a radiomics model (R-model). A radiomics score (Rad-score) was calculated for each patient via a linear combination of selected features that were weighted by their respective coefficients. The workflow is presented in *Figure 1*.

Additionally, the selected clinical characteristics were combined with radiomics features to construct a combined model (RC-model).

Evaluating the performance of the models

The diagnostic performance of the C-model, R-model, and RC-model was assessed according to a receiver operating characteristic (ROC) curve and the area under the ROC curve (AUC) in both the training and validation cohorts.

Accuracy, specificity, and sensitivity were calculated from the threshold values of the maximum Youden index. Decision curve analysis (DCA) was employed to investigate the 3 models through calculating the net benefit for a range of threshold probabilities in the whole cohort. The calibration curve was provided and the Hosmer-Lemeshow (HL) test was used to evaluate the agreement between the true and predicted outcomes of pathology type in pNT. The integrated discrimination improvement (IDI) and net reclassification improvement (NRI) were used to compare the differences in AUC values between different models.

Statistical analysis

All statistical analyses were performed using R (version 4.1.0, statistical computing base). Two-sided P values of less than 0.05 were considered statistically significant. The R packages "glmnet" and "pROC" were used for LASSO binary logistic regression and to construct the ROC curves. The "rms" package was employed to create nomograms. PET/CT radiographic features and clinical parameters were compared between the FH type and the UH type using independent Mann-Whitney U tests and χ^2 tests between the 2 cohorts.

Results

Patient characteristics and clinical model building

The clinical characteristics and radiographic features of the training and validation sets are summarized in *Table 1*. None of these clinical characteristics differed significantly between the training and validation sets. Meaningful characteristics including age, gender, NSE, SF, LDH, SUVmax, INRGSS, infiltration across the midline, and calcification were identified as P<0.05 by univariate analysis. The UH type patients were older; more likely to be female; had higher levels of NSE, SF, LDH, and SUVmax; and were more likely to have a higher INRGSS stage, infiltration across the midline, and calcification.

Three of these factors, age, LDH, and INRGSS stage, were selected using backward stepwise multivariate logistic regression analysis (*Table 2*). Except for MS stage patients, the risk of developing UH type increased with increasing INRGSS stage in all patients. The C-model was then developed based on the independent variables described above. The AUC was 0.856 [95% confidence interval (CI): 0.769–0.944] in the training cohort and 0.803 (95% CI: 0.624–0.981) in the validation cohort (*Table 3* and *Figure 2*).

Construction of the radiomics signature

After univariate analysis, 50 radiomics features (CT: 15, PET: 35) with P<0.05 were retained. Finally, 5 features (4 PET texture features and 1 CT texture feature) used to predict INPC type were selected by LASSO regression (*Figure 3*). A comparison of these features is shown as a heat map in Figure S2. A selected value of λ was used to select features with nonzero coefficients from the coefficient profiles plot (Figure S3). After the number of features was determined, the most predictive subset of features was chosen, and the corresponding coefficients were calculated. Rad-score was calculated by linear combination of the selected features weighted by their coefficients. The Rad-score for each patient was calculated using the following formula:

$$\begin{aligned} Rad\text{-}score = & -0.6268 \\ & \times CT\_wavelet.LHL\_glszm\_size\ zone\ non\ uniformity\ normalized - 0.5267 \\ & \times PET\_original\_shape\_flatness + 0.7287 \\ & \times PET\_wavelet.LHH\_glszm\_gray\ level\ non\ uniformity + 1.0487 \\ & \times PET\_wavelet.HLL\_glcm\_inverse\ variance - 0.6002 \\ & \times PET\_wavelet.HLH\_glszm\_size\ zone\ non\ uniformity\ normalized \end{aligned} \quad [1]$$

The AUC of the R-model was 0.877 (95% CI: 0.801–0.953) in the training cohort and 0.868 (95% CI: 0.735–1.000) in the validation cohort (*Table 3* and *Figure 2*). To illustrate the effectiveness of the R-model, the quantitative values of the models for each pNT patient using the classification of FH and UH type are presented in Figure S4.

After performing multivariate logistic regression analysis, the RC-model was constructed on the basis of age, LDH, INRGSS stage, and Rad-score. The AUC of the RC-model was 0.921 (95% CI: 0.855–0.987) in the training cohort and 0.908 (95% CI: 0.791–1.000) in the validation cohort (*Table 3* and *Figure 2*).

Model comparisons

The IDI and NRI of the 3 models are shown in *Table 4*. According to the IDI index, the predictive ability of the RC-model was better than that of the R-model and C-model, and there were significant differences in the training cohort and validation cohort (all P values <0.05). However, there was no significant difference between the R-model and C-model. According to the NRI index, the predictive performance of the 3 models had the same tendency.

The calibration curve showed that the RC-model and R-model were basically consistent in predicting the INPC type of pNT in the training and validation cohorts,

Table 1 Characteristics of patients with pediatric peripheral neuroblastic tumors in the training set and validation set

Characteristics	Training cohort (n=75)			Validation cohort (n=31)		
	FH (n=28)	UH (n=47)	P value	FH (n=12)	UH (n=19)	P value
Age (years), median [IQR]	1.600 [1.150, 2.700]	3.500 [2.600, 5.050]	<0.001*	1.150 [0.950, 4.575]	4.200 [2.350, 5.250]	0.056
Gender (%)			0.039*			1.000
Male	19 (67.857)	19 (40.426)		9 (75.000)	15 (78.947)	
Female	9 (32.143)	28 (59.574)		3 (25.000)	4 (21.053)	
NSE (ng/mL), median [IQR]	61.300 [28.700, 150.600]	337.900 [164.100, 689.250]	<0.001*	35.850 [18.600, 129.700]	205.970 [93.400, 620.000]	0.004*
SF (ng/mL), median [IQR]	87.600 [29.625, 113.337]	189.500 [105.450, 327.150]	<0.001*	98.719 [62.275, 113.337]	255.105 [114.250, 388.350]	0.010*
LDH (U/L), median [IQR]	354.500 [295.750, 556.250]	753.000 [401.000, 1086.000]	0.005*	303.500 [230.000, 341.000]	577.000 [370.500, 661.000]	0.003*
VMA (μmol/L), median [IQR]	355.227 [50.257, 419.808]	230.461 [41.758, 469.764]	0.767	30.766 [25.995, 355.126]	469.764 [53.902, 469.764]	0.073
HVA (μmol/L), median [IQR]	63.309 [10.476, 81.802]	48.040 [16.310, 127.216]	0.504	7.393 [3.760, 79.051]	127.216 [32.372, 127.216]	0.004*
SUVmax, median [IQR]	4.150 [3.100, 5.375]	5.400 [4.250, 6.650]	0.014*	4.20 [3.275, 5.000]	4.60 [3.800, 6.350]	0.361
TLG, median [IQR]	237.100 [142.925, 403.200]	253.600 [81.050, 574.700]	0.322	182.900 [37.825, 281.325]	294.900 [138.500, 691.450]	0.062
MTV, median [IQR]	108.100 [53.325, 143.875]	123.100 [41.850, 235.400]	0.642	59.750 [17.675, 143.450]	207.100 [47.750, 254.750]	0.039*
INRGSS (%)			<0.001*			<0.001*
L1	8 (28.571)	5 (10.638)		8 (66.667)	2 (10.526)	
L2	5 (17.857)	9 (19.149)		1 (8.333)	8 (42.105)	
M	6 (21.429)	31 (65.957)		1 (8.333)	9 (47.368)	
MS	9 (32.143)	2 (4.255)		2 (16.667)	0 (0.000)	
Anatomic (%)			0.761			0.148
Chest	4 (14.286)	5 (10.638)		0 (0.000)	4 (21.053)	
Abdomen	19 (67.857)	35 (74.468)		8 (66.667)	12 (63.158)	
Pelvis	2 (7.143)	1 (2.128)		2 (16.667)	0 (0.000)	
Junction	3 (10.714)	6 (12.766)		2 (16.667)	3 (15.789)	
Infiltration across midline (%)			0.004*			0.240
Yes	8 (28.571)	31 (65.957)		10 (83.333)	11 (57.895)	
No	20 (71.429)	16 (34.043)		2 (16.667)	8 (42.105)	
Calcification (%)			0.020*			0.012*
Yes	14 (50.000)	37 (78.723)		5 (41.667)	17 (89.474)	
No	14 (50.000)	10 (21.277)		7 (58.333)	2 (10.526)	
Necrosis (%)			0.823			0.447
Yes	20 (71.429)	36 (76.596)		7 (58.333)	14 (73.684)	
No	8 (28.571)	11 (23.404)		5 (41.667)	5 (26.316)	

*, statistical difference. FH, favorable histology; UH, unfavorable histology; IQR, interquartile range; NSE, neuron-specific enolase; SF, serum ferritin; LDH, lactate dehydrogenase; VMA, vanillylmandelic acid; HVA, homovanillic acid; SUVmax, maximum standardized uptake value; MTV, metabolic tumor volume; TLG, total lesion glycolysis; INRGSS, International Neuroblastoma Risk Group Staging System.

Table 2 Univariate and multivariate logistic regression analysis in the cohort

Characteristics	Univariate analysis		Multivariate analysis	
	OR (95% CI)	P value	OR (95% CI)	P value
Age (years)	2.176 (1.418, 3.339)	<0.001*	1.341 (1.004, 1.873)	0.062
Gender (male)	3.042 (1.151, 8.536)	0.024*	NA	NA
NSE (ng/mL)	1.003 (1.001, 1.005)	0.003*	NA	NA
SF (ng/mL)	1.004 (1.000, 1.008)	0.038*	NA	NA
LDH (U/L)	1.001 (1.000, 1.002)	0.033*	2.053 (0.757, 6.616)	0.188
SUVmax	1.199 (0.972, 1.478)	0.090*	NA	NA
INRGSS				
L1	Ref	Ref	Ref	Ref
L2	2.734 (0.573, 14.613)	0.211	2.471 (0.521, 12.122)	0.253
M	7.710 (1.905, 35.596)	0.004*	4.534 (0.976, 23.769)	0.060
MS	0.382 (0.040, 2.464)	0324	0.300 (0.026, 2.484)	0.287
Infiltration across midline	4.691 (1.732, 13.780)	0.002*	NA	NA
Calcification	3.610 (1.310, 10.417)	0.013*	NA	NA
Rad-score	NA	NA	2.066 (1.356, 3.440)	0.002*

*, statistical difference. OR, odds ratio; CI, confidence interval; NSE, neuron-specific enolase; SF, serum ferritin; LDH, lactate dehydrogenase; SUVmax, maximum standardized uptake value; INRGSS, International Neuroblastoma Risk Group Staging System; NA, not applicable; L1: localized tumor not involving vital structures as defined by the list of image-defined risk factors and confined to one body compart men; L2: locoregional tumor with presence of one or more image-defined risk factors; M: distant metastatic disease (except stage MS); MS: metastatic disease in children younger than 18 months with metastases confined to skin, liver, and/or bone marrow.

and were better than the C-model. The HL test yielded nonsignificant P values, suggesting no departure from the perfect fit (*Figure 4*). With a threshold probability of 10–80%, DCA revealed that the RC-model was more clinically useful than were the C-model and R-model in the training and validation cohorts (*Figure 5*). To provide a visualized outcome measure, a nomogram figure was plotted for the RC-model (*Figure 6*).

Discussion

This present study demonstrates that ^{18}F-FDG PET/CT-based radiomics models have promising prospects for noninvasively predicting INPC type in pediatric pNT. The RC-model had better predictive performance than did the C-model alone, with AUC values improving from 0.86 to 0.92 for the training cohort and from 0.80 to 0.91 for the test cohort. INPC type determined by noninvasive methods like imaging can avoid complications of invasive biopsies, such as bleeding, infection, and tumor spread, and can also prevent biopsy specimens from affecting the assessment of the accuracy of tumor grading (22).

PNT is a heterogeneous embryonic neural crest cell tumor that often presents as a mass in the neck, chest, abdomen, retroperitoneum, or pelvis. Definitive diagnosis requires a tumor sample via biopsy. Thus far, several methods for obtaining samples from primary tumors have been reported (23). They range from minimally invasive procedures such as ultrasound-guided core needle biopsy, laparoscopy-assisted core needle biopsy, and thoracoscopic/laparoscopic incisional biopsy, to invasive procedures, such as open incisional biopsy. As molecular markers including tumor ploidy, gene amplification, and INPC are becoming increasingly important in the prognosis of neuroblastoma, adequate percutaneous core needle biopsy or incisional biopsy analysis of tissue samples is required. Core needle biopsy has met with some resistance to incorporation into routine clinical practice, with possible explanations including the need for sedation, the number of core needles assumed to be required for small tumors in children, differences in

Table 3 Predictive performances of the C-model, R-model, and RC-model in the training cohort and validation cohort

Models	Training cohort						Validation cohort					
	AUC (95% CI)	ACC (95% CI)	SEN (95% CI)	SPE (95% CI)	PPV (95% CI)	NPV (95% CI)	AUC (95% CI)	ACC (95% CI)	SEN (95% CI)	SPE (95% CI)	PPV (95% CI)	NPV (95% CI)
C-model	0.856 (0.769, 0.944)	0.936 (0.595, 1.000)	0.643 (0.357, 0.786)	0.643 (0.357, 0.786)	0.815 (0.737, 0.825)	0.857 (0.769, 0.880)	0.803 (0.624, 0.981)	0.710 (0.520, 0.858)	0.789 (0.630, 1.000)	0.583 (0.417, 0.919)	0.750 (0.705, 0.792)	0.636 (0.556, 0.734)
R-model	0.877 (0.801, 0.953)	0.813 (0.707, 0.894)	0.787 (0.532, 0.894)	0.857 (0.500, 0.964)	0.902 (0.862, 0.913)	0.706 (0.583, 0.730)	0.868 (0.735, 1.000)	0.806 (0.625, 0.925)	0.737 (0.474, 1.000)	0.917 (0.500, 1.000)	0.933 (0.900, 0.950)	0.688 (0.545, 0.706)
RC-model	0.921 (0.855, 0.987)	0.893 (0.801, 0.953)	0.936 (0.511, 1.000)	0.821 (0.571, 0.929)	0.898 (0.828, 0.904)	0.885 (0.842, 0.897)	0.908 (0.791, 1.000)	0.903 (0.742, 0.980)	0.895 (0.474, 1.000)	0.917 (0.000, 1.000)	0.944 (0.900, 0.950)	0.846 (0.000, 0.857)

R-model, radiomics model; C-model, clinical model; RC-model, combination model; AUC, area under the curve; CI, confidence interval; ACC, accuracy; SEN, sensitivity; SPE, specificity; PPV, positive predictive value; NPV, negative predictive value.

information obtained from percutaneous core needle biopsy versus surgical biopsy, and the need to weigh the risks of intraoperative complications, infection, and total tumor leakage (24-26). Other perioperative complications include duodenal perforation, pleural effusion, and postoperative hematuria (27). Moreover, the INPC type is based on age, presence of Schwannian stroma, grade of neuroblastic differentiation, and mitosis-karyorrhexis index. The whole process of INPC type classification is complicated, invasive, and expensive. Therefore, based on this study, we believe that the INPC type can be accurately predicted before surgery in a noninvasive manner based on ^{18}F-FDG PET/CT.

In the present study, radiomics features were based on ^{18}F-FDG PET/CT rather than on [^{123}I]MIBG (metaiodobenzylguanidine) SPECT/CT. Currently, ^{123}I-MIBG is the most commonly used imaging modality and is considered the standard of care for patients with pNT. In comparison with ^{18}F-FDG PET/CT, ^{123}I-MIBG scans are carried out over 2 days and have reduced resolution compared to ^{18}F-FDG PET/CT images, which may pose a challenge to inexperienced physicians (28). In many centers, planar I-MIBG imaging scans have been performed, but radiomics based on these images is very limited. In addition, one study suggested that MIBG scans may produce false negatives, which may lead to incorrect downstaging (29).

In about 8% of patients with pNT, false-negative scans are seen at diagnosis despite conclusive evidence of disease. ^{18}F-FDG PET/CT describes the metabolic state of cancer cells, and many studies (30,31) have investigated its value in pNT. In patients with pNT, ^{18}F-FDG PET/CT is more sensitive to the detection of primary and/or residual stage 1 and 2 lesions, as it is more widely available. Liu *et al.* (32) showed that pretherapeutic F-DOPA and F-FDG PET provided complementary information, and both can be used for risk stratification. Overall, ^{18}F-FDG PET/CT is superior in depicting pNT.

In the present study, clinical parameters (age, gender, NSE, SF, and LDH) and radiographic features (SUVmax, infiltration across the midline, and calcification) had statistical significance between the FH and UH types. Age has been used as a prognostic factor for patients with pNT. The latest analysis by Sano *et al.* (31) disclosed a cutoff of around 18 months for the optimal prognostic distinction. This is consistent with our current study, as age greater than 18 months indicated a greater probability of INPC classification as UH. NSE is able to detect 42% of localized relapses, 77% of combined local/metastatic relapses,

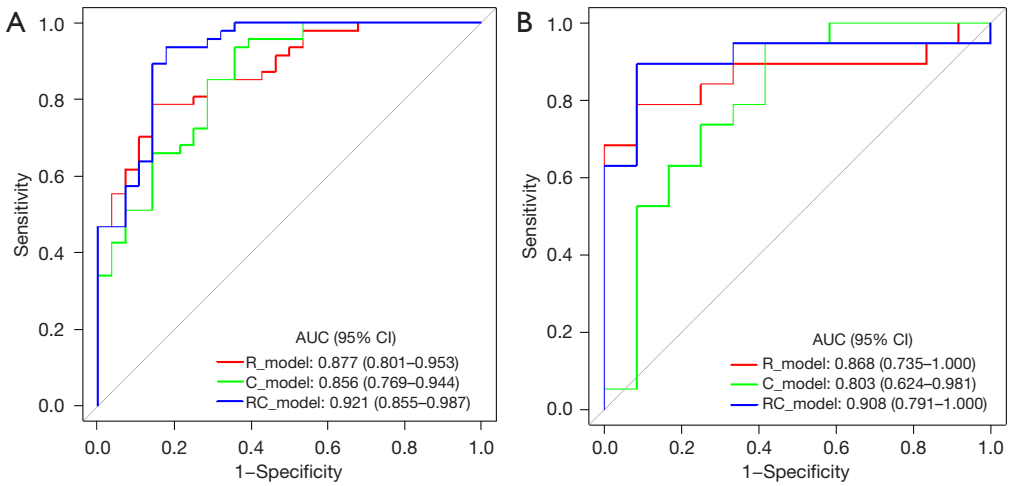

Figure 2 The ROCs used for data analysis in this study. (A) The ROCs of the R-model, C-model, and RC-model in the training cohort. (B) The ROCs of the R-model, C-model, and RC-model in the validation cohort. AUC, area under the curve; CI, confidence interval; R-model, radiomics model; C-model, clinical model; RC-model, combination model; ROC, receiver operating characteristic.

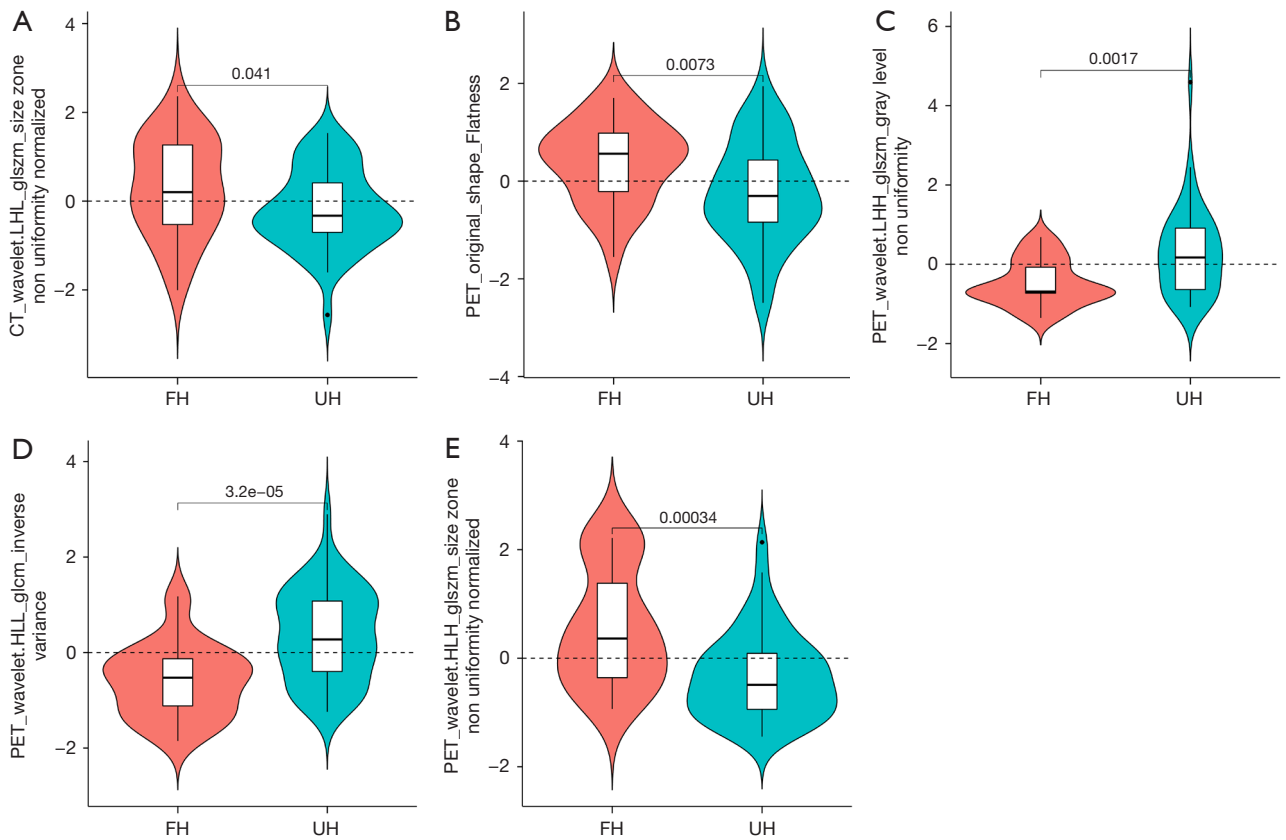

Figure 3 The primary radiomics features extracted in this study. (A) The CT radiomics feature. (B-E) The PET radiomics features. CT, computed tomography; PET, positron emission tomography; FH, favorable histology; UH, unfavorable histology.

Table 4 The IDI and NRI indexes between different models

Models	Training cohort				Validation cohort			
	IDI (95% CI)	P value	NRI (95% CI)	P value	IDI (95% CI)	P value	NRI (95% CI)	P value
R-model *vs.* C-model	0.033 (–0.089, 0.155)	0.595	0.008 (–0.226, 0.241)	0.949	-0.013 (–0.278, 0.251)	0.921	0.189 (–0.251, 0.628)	0.400
RC-model *vs.* R-model	0.110 (0.028, 0.192)	0.009	0.221 (0.012, 0.430)	0.038	0.206 (0.082, 0.330)	0.001	0.618 (0.291, 0.946)	<0.001
RC-model *vs.* C-model	0.143 (0.054, 0.232)	0.002	0.484 (0.212, 0.756)	<0.001	0.192 (–0.014, 0.399)	0.068	0.439 (0.1047, 0.773)	0.01

IDI, integrated discrimination improvement; NRI, net reclassification improvement; CI, confidence interval; R-model, radiomics model; C-model, clinical model; RC-model, combination model.

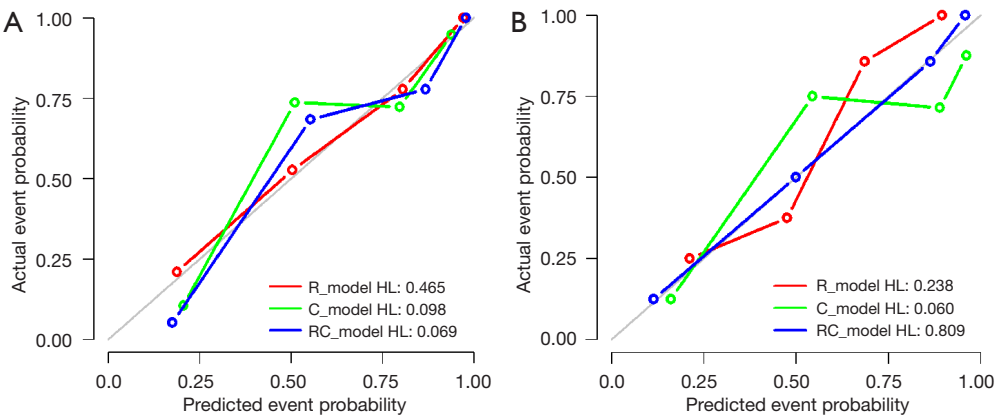

Figure 4 The calibration curves used for data analysis in this study. (A) The calibration curves for the R-model, C-model, and RC-model in the training cohort. (B) The calibration curves for the R-model, C-model, and RC-model in the validation cohort. R-model, radiomics model; C-model, clinical model; RC-model, combination model; HL, Hosmer-Lemeshow.

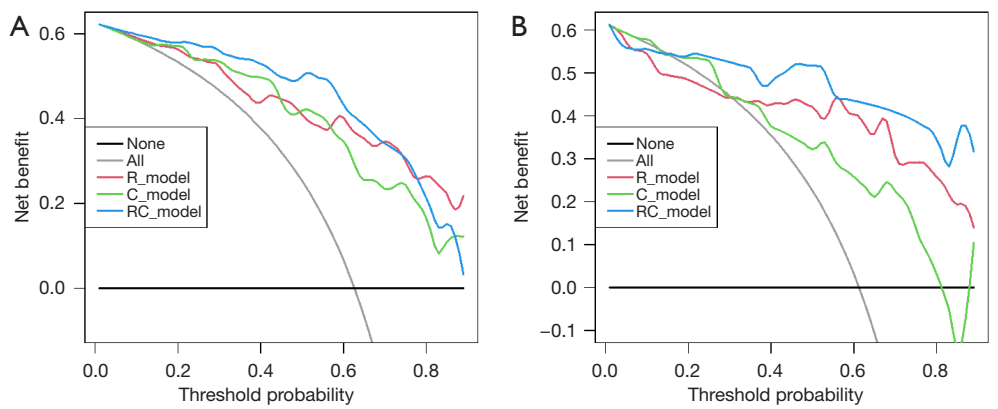

Figure 5 The decision curve analysis in this study. (A) The decision curve analysis for the R-model, C-model, and RC-model in the training cohort. (B) The decision curve analysis for the R-model, C-model, and RC-model in the validation cohort. R-model, radiomics model; C-model, clinical model; RC-model, combination model.

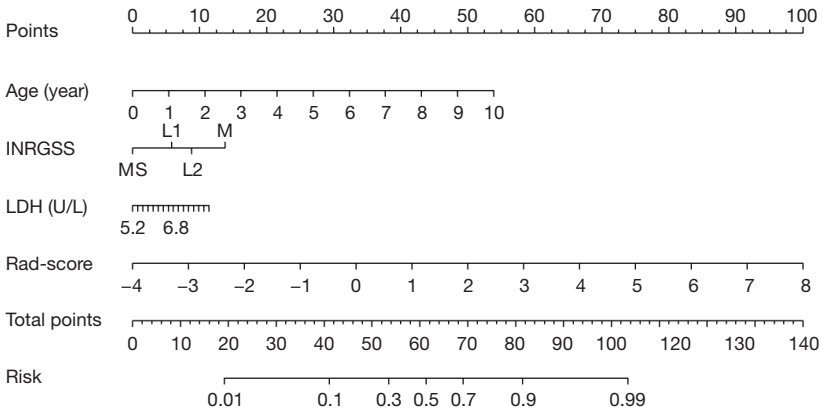

Figure 6 The RC-model nomogram was developed for the prediction of unfavorable histology pNT type using age, INRGSS, LDH, and Rad-score. To use this nomogram, first locate the patient's age, then draw a line straight up to the point's axis on the top to obtain the score associated with age. Repeat the process for the other covariates (from age to Rad-score value). Add the score of each covariate together and locate the total score on the total points axis just below the last covariate–Bovine arch axis. Next, draw a line straight down to assess the unfavorable histology type risk of pNT. INRGSS, International Neuroblastoma Risk Group Staging System; LDH, lactate dehydrogenase; RC-model, combination model; pNT, peripheral neuroblastic tumor.

and 69% of metastatic recurrences (33). The association between NSE level and INPC type has been investigated previously. Some studies reported a significant correlation between NSE level and patient prognosis, with a high serum level of NSE and strong 123I-MIBG uptake each being predictive of UH of neuroblastoma (34). In our paper, UH type had a higher serum NSE level, which corresponds to the results of the Lau's study (34). He *et al.*'s also found that LDH and SF had a strong prognostic impact on pNT, and they can be used to identify those ultra-high-risk patients, thus refining risk stratification (35). Patients with low SUVmax on PET/CT may have a better prognosis in subsequent treatment, which provides reliable prognostic information for pretreatment pNT patients (36). INRGSS allows for the preoperative risk stratification of patients with pNT (14). Finally, in our study, the 3 clinical characteristics of age, NSE, and INRGSS were used to predict INPC type.

Based on the present research, we discovered radiomics features that can predict the INPC type independent of other clinical parameters and radiographic features. It is possible that these radiomics differences reflect inherent biological tumor differences. We selected 5 radiomics features to establish an RC-model that showed favorable discrimination in predicting the INPC type. This model included 4 PET radiomics features and 1 CT radiomics feature, highlighting the importance of PET radiomics features in the prediction model. A plausible explanation is that PET images allow better monitoring of the tumor microenvironment, and therefore more signal differences can be observed (33).

The IDI index was measured to evaluate the incremental predictive utility of different models. The RC-model was improved by 11.0% compared with the R-model in the training cohort and 20.6% in the validation cohort. The RC-model was improved by 14.3% compared with the C-model in the training cohort and 19.2% in the validation cohort. All the P values showed a significant improvement in reclassification. In the DCA, the RC-model nomogram diagnostic model not only achieved higher diagnostic efficiency and greater net benefit across the entire range of threshold probabilities, but also visualized and personalized the probability of the occurrence of the INPC UH type for each patient.

There are several limitations to this study. First, this was a retrospective study conducted at a single institution, and case selection bias appears to be inevitable. Furthermore, although 106 cases of pNT were included in our study, our sample size remains modest for a radiological study given the heterogeneous disease distribution of pNT. Second, our validation set used to test the effectiveness of the model came from the same hospital as the training set, so it is difficult to generalize our results to other hospitals. Therefore, a large multicenter prospective cohort study is required to validate the results and improve the reliability of the INPC type prediction model in pNT.

In conclusion, the radiomics model may change the systematic treatment or operation plan before the operation. This study is an initial investigation of the radiomics model in INPC classification. The results of the current study have proven to be of interest, as the treatment of neuroblastoma patients can be stratified based on INPC classification and the combination of radiomics features and clinical features allows for a more comprehensive, safer, and cost-effective way of assessing INPC classification preoperatively.

Acknowledgments

Funding: This work was supported by the National Natural Science Foundation of China: Imaging genomics of neuroblastoma based on ^{18}F-FDG PET/CT and ^{123}I-MIBG SPECT/CT (No. 81971642).

Footnote

Reporting Checklist: The authors have completed the STARD reporting checklist. Available at https://qims.amegroups.com/article/view/10.21037/qims-22-343/rc

Conflicts of Interest: All authors have completed the ICMJE uniform disclosure form (available at https://qims.amegroups.com/article/view/10.21037/qims-22-343/coif). The authors report that this work was supported by the National Natural Science Foundation of China: Imaging genomics of neuroblastoma based on ^{18}F-FDG PET/CT and ^{123}I-MIBG SPECT/CT (No. 81971642). JLR is in partnership with GE Healthcare China. LL is in partnership with Sinounion Medical Technology (Beijing) Co., Ltd., Beijing. The authors have no other conflicts of interest to declare.

Ethical Statement: The authors are accountable for all aspects of the work in ensuring that questions related to the accuracy or integrity of any part of the work are appropriately investigated and resolved. The study was conducted in accordance with the Declaration of Helsinki (as revised in 2013). This retrospective study was approved by the Institutional Ethics Committee of Beijing Friendship Hospital, and individual consent for this retrospective analysis was waived.

References

1. Peuchmaur M, d'Amore ES, Joshi VV, Hata J, Roald B, Dehner LP, Gerbing RB, Stram DO, Lukens JN, Matthay KK, Shimada H. Revision of the International Neuroblastoma Pathology Classification: confirmation of favorable and unfavorable prognostic subsets in ganglioneuroblastoma, nodular. Cancer 2003;98:2274-81.
2. Nakazawa A. Biological categories of neuroblastoma based on the international neuroblastoma pathology classification for treatment stratification. Pathol Int 2021;71:232-44.
3. Sokol E, Desai AV, Applebaum MA, Valteau-Couanet D, Park JR, Pearson ADJ, Schleiermacher G, Irwin MS, Hogarty M, Naranjo A, Volchenboum S, Cohn SL, London WB. Age, Diagnostic Category, Tumor Grade, and Mitosis-Karyorrhexis Index Are Independently Prognostic in Neuroblastoma: An INRG Project. J Clin Oncol 2020;38:1906-18.
4. Irwin MS, Park JR. Neuroblastoma: paradigm for precision medicine. Pediatr Clin North Am 2015;62:225-56.
5. Strother DR, London WB, Schmidt ML, Brodeur GM, Shimada H, Thorner P, Collins MH, Tagge E, Adkins S, Reynolds CP, Murray K, Lavey RS, Matthay KK, Castleberry R, Maris JM, Cohn SL. Outcome after surgery alone or with restricted use of chemotherapy for patients with low-risk neuroblastoma: results of Children's Oncology Group study P9641. J Clin Oncol 2012;30:1842-8.
6. Maris JM, Hogarty MD, Bagatell R, Cohn SL. Neuroblastoma. Lancet 2007;369:2106-20.
7. Santiago T, Polanco AC, Fuentes-Alabi S, Hayes C, Orellana E, Gomero B, González MT, Ruiz E, Durán ME, Rodriguez-Galindo C, Metzger M. Multinational Retrospective Central Pathology Review of Neuroblastoma: Lessons Learned to Establish a Regional Pathology Referral Center in Resource-Limited Settings. Arch Pathol Lab Med 2021;145:214-21.
8. Temple WC, Vo KT, Matthay KK, Balliu B, Coleman C, Michlitsch J, Phelps A, Behr S, Zapala MA. Association of image-defined risk factors with clinical features, histopathology, and outcomes in neuroblastoma. Cancer Med 2021;10:2232-41.

9. Jansen RW, van Amstel P, Martens RM, Kooi IE, Wesseling P, de Langen AJ, Menke-Van der Houven van Oordt CW, Jansen BHE, Moll AC, Dorsman JC, Castelijns JA, de Graaf P, de Jong MC. Non-invasive tumor genotyping using radiogenomic biomarkers, a systematic review and oncology-wide pathway analysis. Oncotarget 2018;9:20134-55.
10. Hatt M, Tixier F, Pierce L, Kinahan PE, Le Rest CC, Visvikis D. Characterization of PET/CT images using texture analysis: the past, the present… any future? Eur J Nucl Med Mol Imaging 2017;44:151-65.
11. Ding J, Xing Z, Jiang Z, Chen J, Pan L, Qiu J, Xing W. CT-based radiomic model predicts high grade of clear cell renal cell carcinoma. Eur J Radiol 2018;103:51-6.
12. Li Z, Kaiser L, Holzgreve A, Ruf VC, Suchorska B, Wenter V, Quach S, Herms J, Bartenstein P, Tonn JC, Unterrainer M, Albert NL. Prediction of TERTp-mutation status in IDH-wildtype high-grade gliomas using pre-treatment dynamic 18FFET PET radiomics. Eur J Nucl Med Mol Imaging 2021;48:4415-25.
13. Jiang C, Zhao L, Xin B, Ma G, Wang X, Song S. 18F-FDG PET/CT radiomic analysis for classifying and predicting microvascular invasion in hepatocellular carcinoma and intrahepatic cholangiocarcinoma. Quant Imaging Med Surg 2022;12:4135-50.
14. Umutlu L, Kirchner J, Bruckmann NM, Morawitz J, Antoch G, Ingenwerth M, Bittner AK, Hoffmann O, Haubold J, Grueneisen J, Quick HH, Rischpler C, Herrmann K, Gibbs P, Pinker-Domenig K. Multiparametric Integrated 18F-FDG PET/MRI-Based Radiomics for Breast Cancer Phenotyping and Tumor Decoding. Cancers (Basel) 2021;13:2928.
15. Stauss J, Franzius C, Pfluger T, Juergens KU, Biassoni L, Begent J, Kluge R, Amthauer H, Voelker T, Højgaard L, Barrington S, Hain S, Lynch T, Hahn K; European Association of Nuclear Medicine. Guidelines for 18F-FDG PET and PET-CT imaging in paediatric oncology. Eur J Nucl Med Mol Imaging 2008;35:1581-8.
16. Delbeke D, Coleman RE, Guiberteau MJ, Brown ML, Royal HD, Siegel BA, Townsend DW, Berland LL, Parker JA, Hubner K, Stabin MG, Zubal G, Kachelriess M, Cronin V, Holbrook S. Procedure guideline for tumor imaging with 18F-FDG PET/CT 1.0. J Nucl Med 2006;47:885-95.
17. Monclair T, Brodeur GM, Ambros PF, Brisse HJ, Cecchetto G, Holmes K, Kaneko M, London WB, Matthay KK, Nuchtern JG, von Schweinitz D, Simon T, Cohn SL, Pearson AD; INRG Task Force. The International Neuroblastoma Risk Group (INRG) staging system: an INRG Task Force report. J Clin Oncol 2009;27:298-303.
18. Guezennec C, Robin P, Orlhac F, Bourhis D, Delcroix O, Gobel Y, Rousset J, Schick U, Salaün PY, Abgral R. Prognostic value of textural indices extracted from pretherapeutic 18-F FDG-PET/CT in head and neck squamous cell carcinoma. Head Neck 2019;41:495-502.
19. Abgral R, Valette G, Robin P, Rousset J, Keromnes N, Le Roux PY, Marianowski R, Salaün PY. Prognostic evaluation of percentage variation of metabolic tumor burden calculated by dual-phase (18) FDG PET-CT imaging in patients with head and neck cancer. Head Neck 2016;38 Suppl 1:E600-6.
20. Dibble EH, Alvarez AC, Truong MT, Mercier G, Cook EF, Subramaniam RM. 18F-FDG metabolic tumor volume and total glycolytic activity of oral cavity and oropharyngeal squamous cell cancer: adding value to clinical staging. J Nucl Med 2012;53:709-15.
21. Nioche C, Orlhac F, Boughdad S, Reuzé S, Goya-Outi J, Robert C, Pellot-Barakat C, Soussan M, Frouin F, Buvat I. LIFEx: A Freeware for Radiomic Feature Calculation in Multimodality Imaging to Accelerate Advances in the Characterization of Tumor Heterogeneity. Cancer Res 2018;78:4786-9.
22. Yi X, Xiao Q, Zeng F, Yin H, Li Z, Qian C, Wang C, Lei G, Xu Q, Li C, Li M, Gong G, Zee C, Guan X, Liu L, Chen BT. Computed Tomography Radiomics for Predicting Pathological Grade of Renal Cell Carcinoma. Front Oncol 2021;10:570396.
23. Metz T, Heider A, Vellody R, Jarboe MD, Gemmete JJ, Grove JJ, Smith EA, Mody R, Newman EA, Dillman JR. Image-guided percutaneous core needle biopsy of soft-tissue masses in the pediatric population. Pediatr Radiol 2016;46:1173-8.
24. Sklair-Levy M, Lebensart PD, Applbaum YH, Ramu N, Freeman A, Gozal D, Gross E, Sherman Y, Bar-Ziv J, Libson E. Percutaneous image-guided needle biopsy in children--summary of our experience with 57 children. Pediatr Radiol 2001;31:732-6.
25. Hussain HK, Kingston JE, Domizio P, Norton AJ, Reznek RH. Imaging-guided core biopsy for the diagnosis of malignant tumors in pediatric patients. AJR Am J Roentgenol 2001;176:43-7.
26. Paraboschi I, Bolognesi E, Giannettoni A, Avanzini S, Torre M, Martucciello G. The Role of Biopsy in the Workup of Patients with Neuroblastoma: Comparison of the Incidence of Surgical Complications and the

Diagnostic Reliability of Diverse Techniques. Children (Basel) 2021;8:500.
27. Wen Z, Zhang L, Zhuang H. Roles of PET/Computed Tomography in the Evaluation of Neuroblastoma. PET Clin 2020;15:321-31.
28. Bleeker G, Tytgat GA, Adam JA, Caron HN, Kremer LC, Hooft L, van Dalen EC. 123I-MIBG scintigraphy and 18F-FDG-PET imaging for diagnosing neuroblastoma. Cochrane Database Syst Rev 2015;2015:CD009263.
29. Melzer HI, Coppenrath E, Schmid I, Albert MH, von Schweinitz D, Tudball C, Bartenstein P, Pfluger T. ^{123}I-MIBG scintigraphy/SPECT versus ^{18}F-FDG PET in paediatric neuroblastoma. Eur J Nucl Med Mol Imaging 2011;38:1648-58.
30. Sharp SE, Shulkin BL, Gelfand MJ, Salisbury S, Furman WL. 123I-MIBG scintigraphy and 18F-FDG PET in neuroblastoma. J Nucl Med 2009;50:1237-43.
31. Sano H, Bonadio J, Gerbing RB, London WB, Matthay KK, Lukens JN, Shimada H. International neuroblastoma pathology classification adds independent prognostic information beyond the prognostic contribution of age. Eur J Cancer 2006;42:1113-9.
32. Liu CJ, Lu MY, Liu YL, Ko CL, Ko KY, Tzen KY, Chang HH, Yang YL, Jou ST, Hsu WM, Yen RF. Risk Stratification of Pediatric Patients With Neuroblastoma Using Volumetric Parameters of 18F-FDG and 18F-DOPA PET/CT. Clin Nucl Med 2017;42:e142-8.
33. Fendler WP, Wenter V, Thornton HI, Ilhan H, von Schweinitz D, Coppenrath E, Schmid I, Bartenstein P, Pfluger T. Combined Scintigraphy and Tumor Marker Analysis Predicts Unfavorable Histopathology of Neuroblastic Tumors with High Accuracy. PLoS One 2015;10:e0132809.
34. Lau L. Neuroblastoma: a single institution's experience with 128 children and an evaluation of clinical and biological prognostic factors. Pediatr Hematol Oncol 2002;19:79-89.
35. He WG, Yan Y, Tang W, Cai R, Ren G. Clinical and biological features of neuroblastic tumors: A comparison of neuroblastoma and ganglioneuroblastoma. Oncotarget 2017;8:37730-9.
36. Li C, Zhang J, Chen S, Huang S, Wu S, Zhang L, Zhang F, Wang H. Prognostic value of metabolic indices and bone marrow uptake pattern on preoperative 18F-FDG PET/CT in pediatric patients with neuroblastoma. Eur J Nucl Med Mol Imaging 2018;45:306-15.

Cite this article as: Qian LD, Feng LJ, Zhang SX, Liu J, Ren JL, Liu L, Zhang H, Yang J. ^{18}F-FDG PET/CT imaging of pediatric peripheral neuroblastic tumor: a combined model to predict the International Neuroblastoma Pathology Classification. Quant Imaging Med Surg 2023;13(1):94-107. doi: 10.21037/qims-22-343

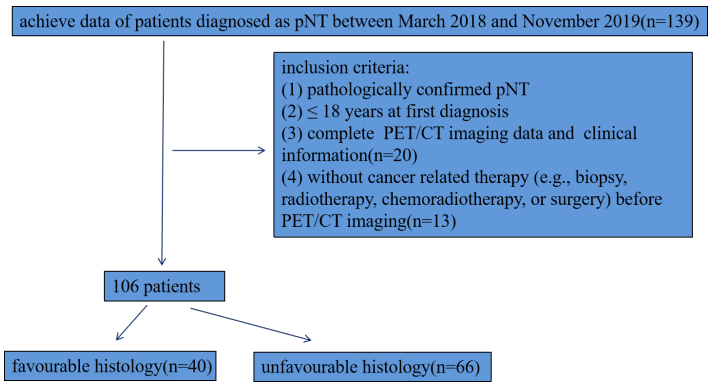

Figure S1 Recruitment pathway for patients in this study.

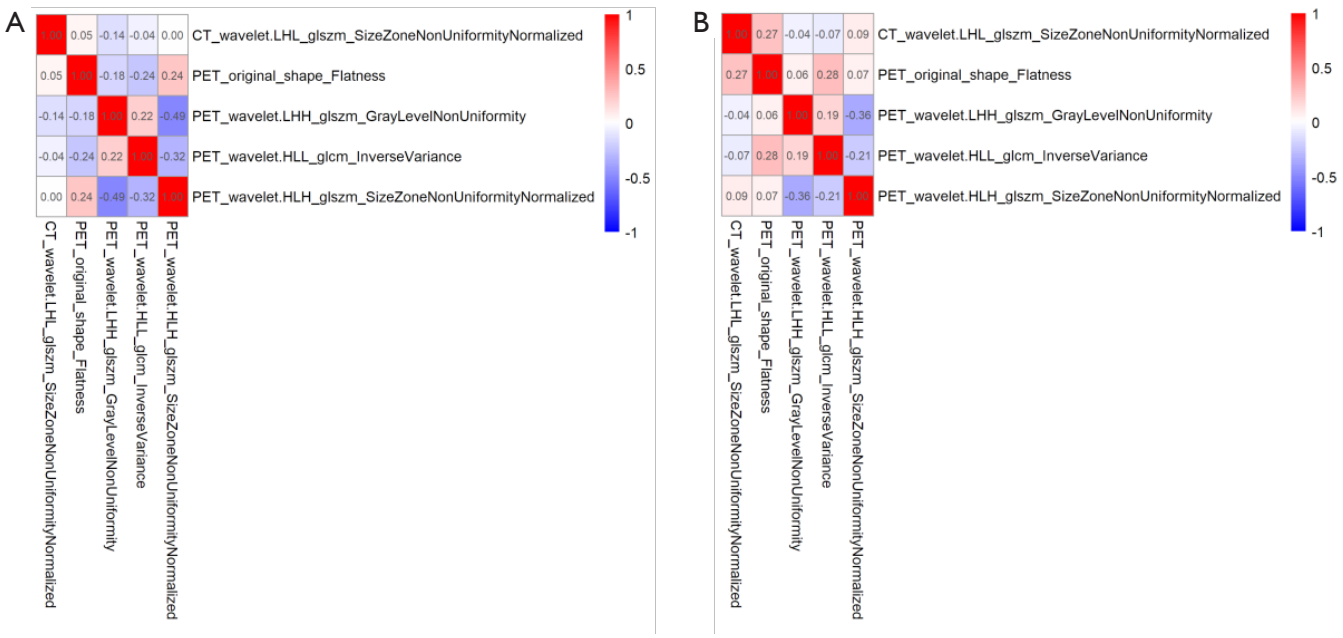

Figure S2 Heatmap comparison of the radiomics features. (A) Training cohort. (B) Validation cohort.

https://dx.doi.org/10.21037/qims-22-343

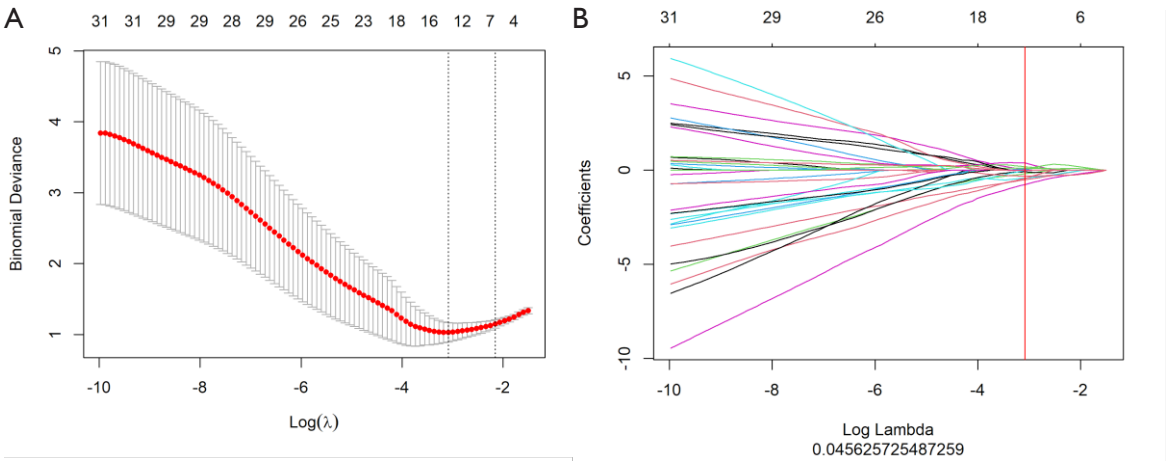

Figure S3 Feature selection using the least absolute shrinkage and selection operator (LASSO) regression algorithm and the performance of radiomics signature. (A) The tuning parameter (λ) in the LASSO model was selected via 10-fold cross-validation based on minimum criteria. The binomial deviance was plotted as a function of log (λ). Dotted red curve indicated the average binominal deviance values for each model with a given λ. The left dotted vertical line defined the optimal values of λ by using the minimum criteria and the 1 standard error of the minimum criteria. The λ value was set as 0.07008150 in this study. (B) The dotted vertical line was plotted at the selected λ value, resulting in 5 non-zero-coefficient features.

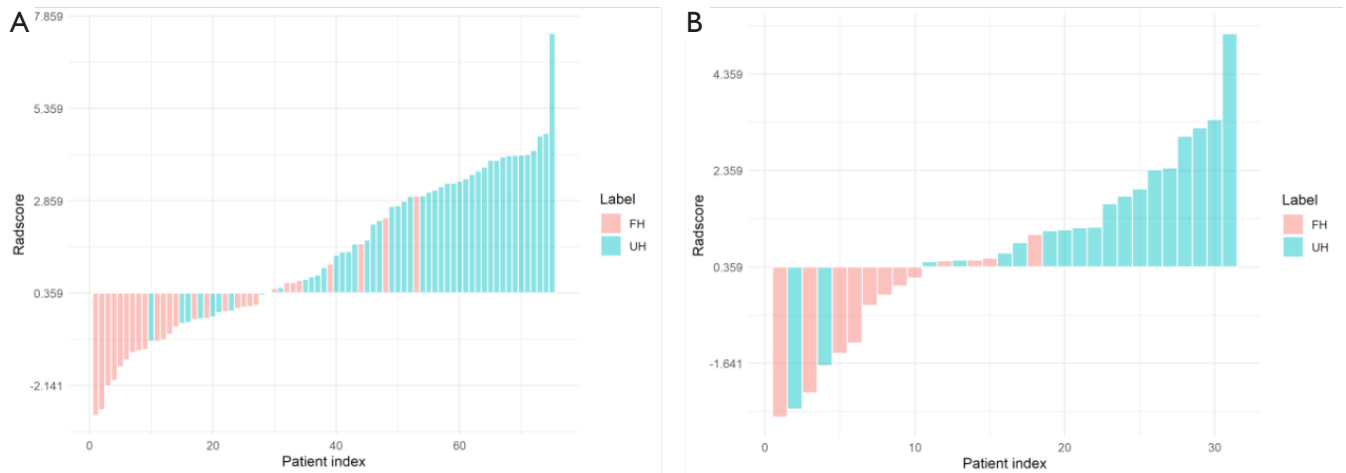

Figure S4 The red bars show the scores for FH type pNTs patients and the blue bars show the scores for UH type pNTs patients. (A) Training cohort. (B) Validation cohort.

https://dx.doi.org/10.21037/qims-22-343